Supplementary Information

1. Supplementary Tables (S1-S6)

Table S1. Antibodies used for immunofluorescence staining

Antibodies	Host	Manufacturer	Cat#
ALB	Mouse	Santa cruz	sc-374670
CLDN5	Mouse	Invitrogen	35-2500
CD4	Mouse	Invitrogen	14-0042-82
GFAP	Mouse	Millipore	MAB360
Iba-1	Rabbit	Wako	019-19741
IFN-γ	Rabbit	Bioss	bs-1183R
IL-17A	Rabbit	Bioss	bs-0480R
MBP	Rat	Abcam	ab7349
OCLN	Mouse	Invitrogen	33-1500
PECAM-1	Mouse	Santa cruz	sc-46694
FITC Goat Anti-Rat IgG	-	Jackson ImmunoResearch	112-095-003
Cy™3 Goat Anti-Mouse IgG	-	Jackson ImmunoResearch	115-165-003
Cy™3 Goat Anti-Rabbit IgG	-	Jackson ImmunoResearch	111-165-003

Table S2. Antibodies used for Western Blotting

Antibodies	Host	Manufacturer	Cat#
β-actin	Mouse	Santa cruz	sc-47778
MBP	Rat	Abcam	ab7349
IBA-1	Rabbit	Wako	019-19741
GFAP	Mouse	Millipore	MAB360
TLR4	Rabbit	IMGENEX	IMG-578A
Myd88	Mouse	Santa cruz	sc-74532
p-NF-κB	Rabbit	Cell Signaling Technology	3033
NF-κB	Mouse	Santa cruz	sc-7151
p-JNK	Rabbit	Cell Signaling Technology	4668

JNK	Rabbit	Cell Signaling Technology	9258
p-ERK	Rabbit	Cell Signaling Technology	4370
ERK	Rabbit	Cell Signaling Technology	4695S
p-p38	Mouse	Cell Signaling Technology	9216
P38	Rabbit	Cell Signaling Technology	9212
PECAM-1	Mouse	Santa cruz	sc-46694
iNOS	Mouse	BD transduction laboratories	610329
Horse Anti-Mouse IgG	-	Vector	BA-2000
Goat Anti-Rabbit IgG	-	Vector	BA-1000
Goat Anti-Rat IgG	-	Vector	BA-9400

Table S3. Primer sequences used for Real-Time Polymerase Chain Reaction

Primers	Forward sequence	Reverse sequence
GAPDH	AGG TCA TCC CAG AGC TGA ACG	CAC CCT GTT GCT GTA GCC GTA T
IL-6	TCC ATC CAG TTG CCT TCT TGG	CCA CGA TTT CCC AGA GAA C
iNOS	GGC AAA CCC AAG GTC TAG GTT	TCG CTC AAG TTC AGC TTG GT
MCP-1	CTT CTG GGC CTG CTG TTC A	CCA GCC TAC TCA TTG GGA TCA
MIP-1α	CAG CCA GGT GTC ATT TTC CT	AGG CAT TCA GTT CCA GGT CA

Table S4. Antibodies used for flow cytometry

Antibodies	Manufacturer	Cat#
PerCP-Cy™5.5 Rat Anti-Mouse CD4	BD biosciences	550954
PE Rat Anti-Mouse CD8a	BD biosciences	561095
APC Anti-Mouse IFN-γ	BioLegend	505809
PE Rat Anti-Mouse IL-17A	BD biosciences	561020

Table S5. Physicochemical properties of IVL4002 microspheres.

Drug	D10 (μm)	D50 (μm)	D90 (μm)	Mean diameter (μm)	CV (%)	Span
IVL4002	47.35	54.88	61.58	54.88	10.41	0.26

Formulation parameter	Value
Encapsulation efficiency (%)	88.97
Residual solvent (ppm)	11

Footnote: Span = (D90 − D10) / D50.

Table S6. Body weight changes in rat and dog toxicity studies.

A. Body weight changes in male rats

Treatment group	Day 1 (g)	Day 8 (g)	Day 15 (g)	Day 22 (g)	Day 29 (g)
Vehicle control	259 ± 25.2	282 ± 15.0	355 ± 26.6	394 ± 33.4	436 ± 40.8
Placebo control	261 ± 26.6	308 ± 29.3	346 ± 32.0	382 ± 31.0	413 ± 32.8
IVL4002 (Low dose)	265 ± 27.1	298 ± 23.8	343 ± 32.6	374 ± 37.3	403 ± 42.4

IVL4002 (High dose)	260 ± 28.3	292 ± 25.7	341 ± 30.1	374 ± 35.7	407 ± 40.1

B. Body weight changes in female rats

Treatment group	Day 1 (g)	Day 8 (g)	Day 15 (g)	Day 22 (g)	Day 29 (g)
Vehicle control	209 ± 17.3	229 ± 16.7	244 ± 15.2	256 ± 18.0	264 ± 17.4
Placebo control	210 ± 17.9	228 ± 23.2	246 ± 30.8	254 ± 32.7	260 ± 32.4
IVL4002 (Low dose)	211 ± 24.4	226 ± 26.7	238 ± 26.9	248 ± 30.7	256 ± 34.5
IVL4002 (High dose)	207 ± 20.0	224 ± 20.4	235 ± 21.9	243 ± 24.7	252 ± 27.2

C. Body weight changes in male dogs

Treatment group	Day 1 (kg)	Day 8 (kg)	Day 15 (kg)	Day 22 (kg)	Day 29 (kg)
Vehicle control	10.13 ± 0.863	10.21 ± 0.988	10.47 ± 0.965	10.25 ± 0.967	10.49 ± 0.980
Placebo control	10.24 ± 0.390	10.11 ± 0.470	10.33 ± 0.290	10.10 ± 0.470	10.38 ± 0.367
IVL4002 (Low dose)	10.18 ± 1.220	10.16 ± 1.269	10.55 ± 1.272	10.39 ± 1.096	10.65 ± 1.002

IVL4002 (High dose)	10.05 ± 0.654	10.19 ± 1.021	10.45 ± 1.011	10.20 ± 1.145	10.25 ± 1.068

D. Body weight changes in female dogs

Treatment group	Day 1 (kg)	Day 8 (kg)	Day 15 (kg)	Day 22 (kg)	Day 29 (kg)
Vehicle control	8.71 ± 1.191	8.73 ± 1.209	8.93 ± 1.187	8.76 ± 1.300	8.83 ± 1.240
Placebo control	8.47 ± 0.463	8.43 ± 0.531	8.37 ± 0.349	8.26 ± 0.350	8.36 ± 0.426
IVL4002 (Low dose)	8.40 ± 0.899	8.53 ± 0.998	8.38 ± 1.179	8.40 ± 1.146	8.42 ± 1.121
IVL4002 (High dose)	8.56 ± 0.601	8.58 ± 0.529	8.59 ± 0.600	8.41 ± 0.416	8.36 ± 0.408

2. Supplementary Figures (S1-S7)

Figure S1

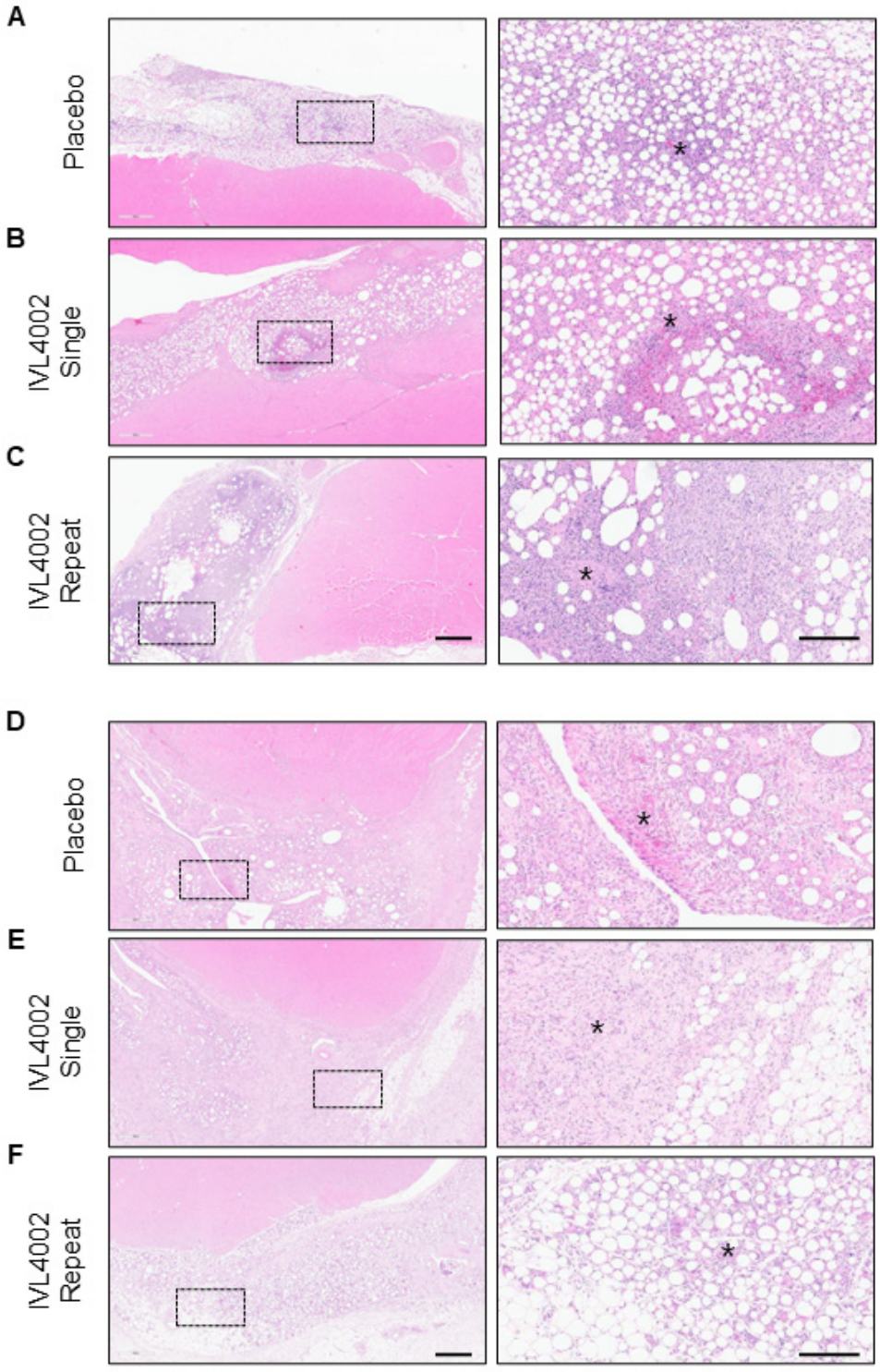


Figure S1. Histopathological evaluation of injection-site tissues following placebo microsphere or IVL4002 administration in rats and dogs. Representative hematoxylin and eosin (H&E)-stained sections of injection-site tissues collected at scheduled necropsy from GLP toxicity studies. **(A–C)** Representative injection-site histopathology in rats treated with placebo microspheres (A), single-dose IVL4002 (B), or repeated-dose IVL4002 (C). Slight granulomatous inflammation was observed across the groups, with mixed inflammatory cell infiltration and hemorrhage additionally observed in the single-dose IVL4002 group. **(D–F)** Representative injection-site histopathology in dogs treated with placebo microspheres (D), single-dose IVL4002 (E), or repeated-dose IVL4002 (F), showing slight granulomatous inflammation. Asterisks indicate representative areas of inflammation.Scale bar: 600 μm (left panels) and 200 μm (right panels).

Figure S2

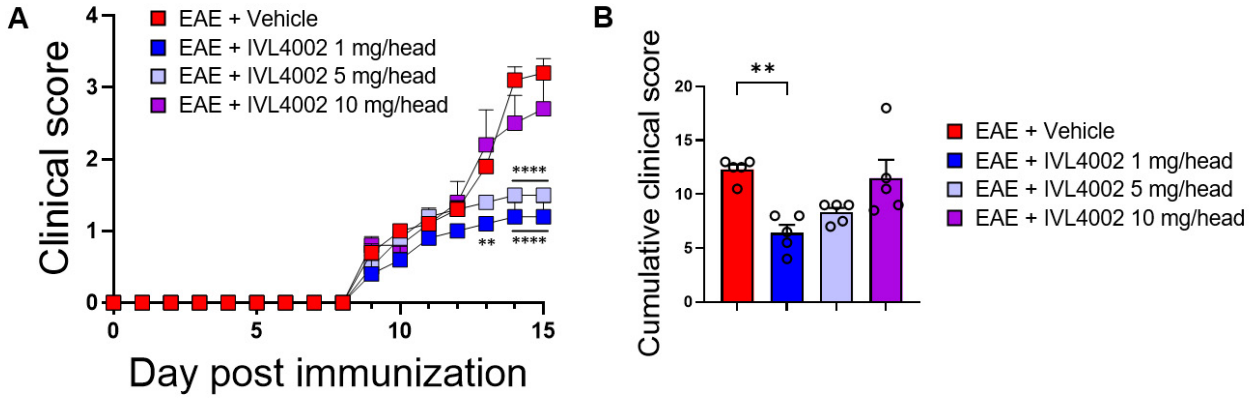


Figure S2. Preliminary dose-finding study of IVL4002 in $MOG_{35–55}$-induced EAE mice. EAE mice received a single subcutaneous administration of vehicle or IVL4002 (1, 5, or 10 mg/head) at 3 days post-immunization. (A) Clinical scores were monitored until day 15 post-immunization. (B) Cumulative clinical scores from days 9 to 15 post-immunization. Among the doses evaluated, IVL4002 at 1 mg/head produced the greatest attenuation of clinical disease severity. Data are presented as the mean ± SEM (n = 5 mice per group). **P < 0.01 and ****P < 0.0001 versus the EAE + vehicle group.

Figure S3

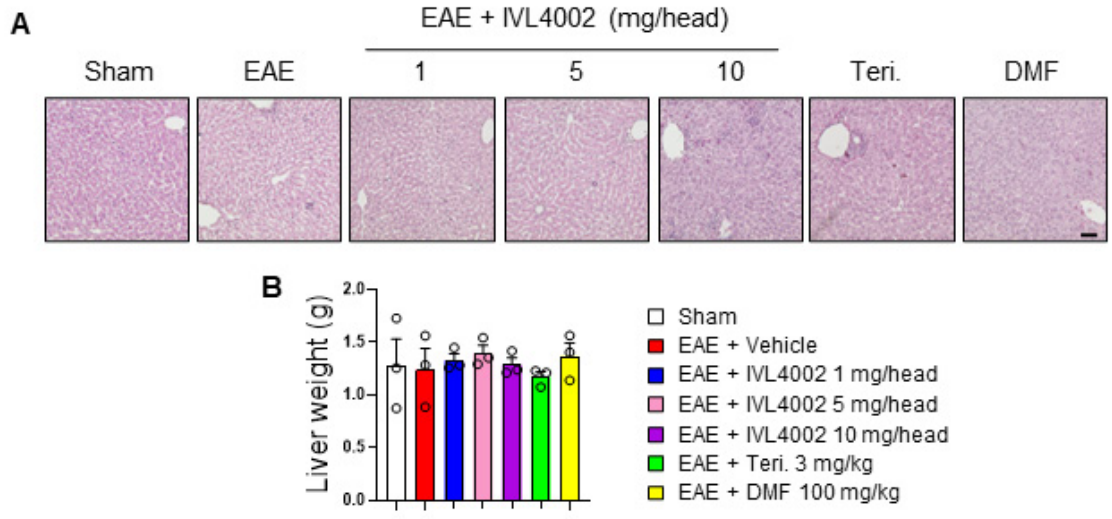


Figure S3. Effects of IVL4002 on liver histology and liver weight in EAE mice. (A) Representative hematoxylin and eosin (H&E)–stained sections of liver tissues obtained from sham, EAE + vehicle, and EAE mice treated with IVL4002 (1, 5, or 10 mg/mL), Teri. (3 mg/kg), or DMF (100 mg/kg). No apparent treatment-related histopathological alterations or inflammatory lesions were observed across groups. **(B)** Quantification of liver weight measured at the experimental endpoint. No significant differences in liver weight were observed among the sham, EAE + vehicle, and treatment groups, indicating that administration of IVL4002 or comparator drugs did not induce detectable hepatic toxicity. Scale bars, 100 μm. Data are presented as mean ± SEM (n = 3 per group). **P* < 0.05, *****P*** < 0.01, ******P*** < 0.001, and *******P*** < 0.0001.

Figure S4

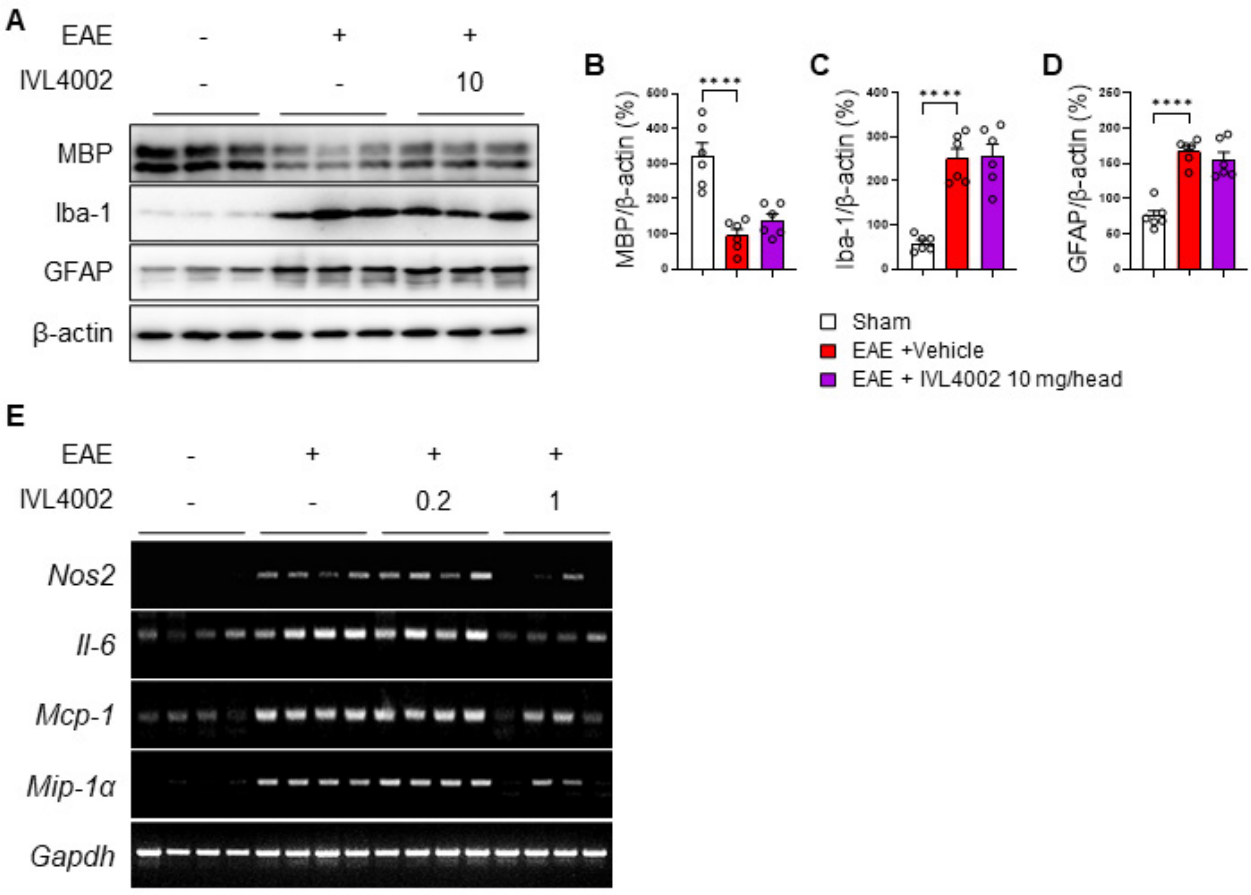


Figure S4. Effects of IVL4002 on glial activation, myelin integrity, and inflammatory gene expression in the spinal cord of EAE mice. (A) Representative Western blot images showing protein expression levels of Iba-1, MBP, and GFAP in lumbar spinal cord tissues from sham, EAE + vehicle, and EAE mice treated with IVL4002 (10 mg/head). β-Actin was used as a loading control. **(B–D)** Densitometric quantification of MBP (B), Iba-1 (C), and GFAP (D) protein expression normalized to β-actin (n = 6 mice per group). **(E)** Representative semi-quantitative RT-PCR bands of *Nos2, Il6, Ccl2*, and *Ccl3* expression in spinal cord tissues corresponding to the quantitative analyses shown in Figure 4H–K. mRNA expression levels of *Nos2*, *Il-6*, *Ccl2 (Mcp-1)*, and *Ccl3* (*Mip-1α*) were examined in sham, EAE + vehicle, and EAE mice treated with IVL4002 (0.2 or 1 mg/head). *Gapdh* was used as an internal control (n = 4 mice per group). Data are presented as mean ± SEM. **P* < 0.05, ***P* < 0.01, ****P* < 0.001, and *****P* < 0.0001.

Figure S5

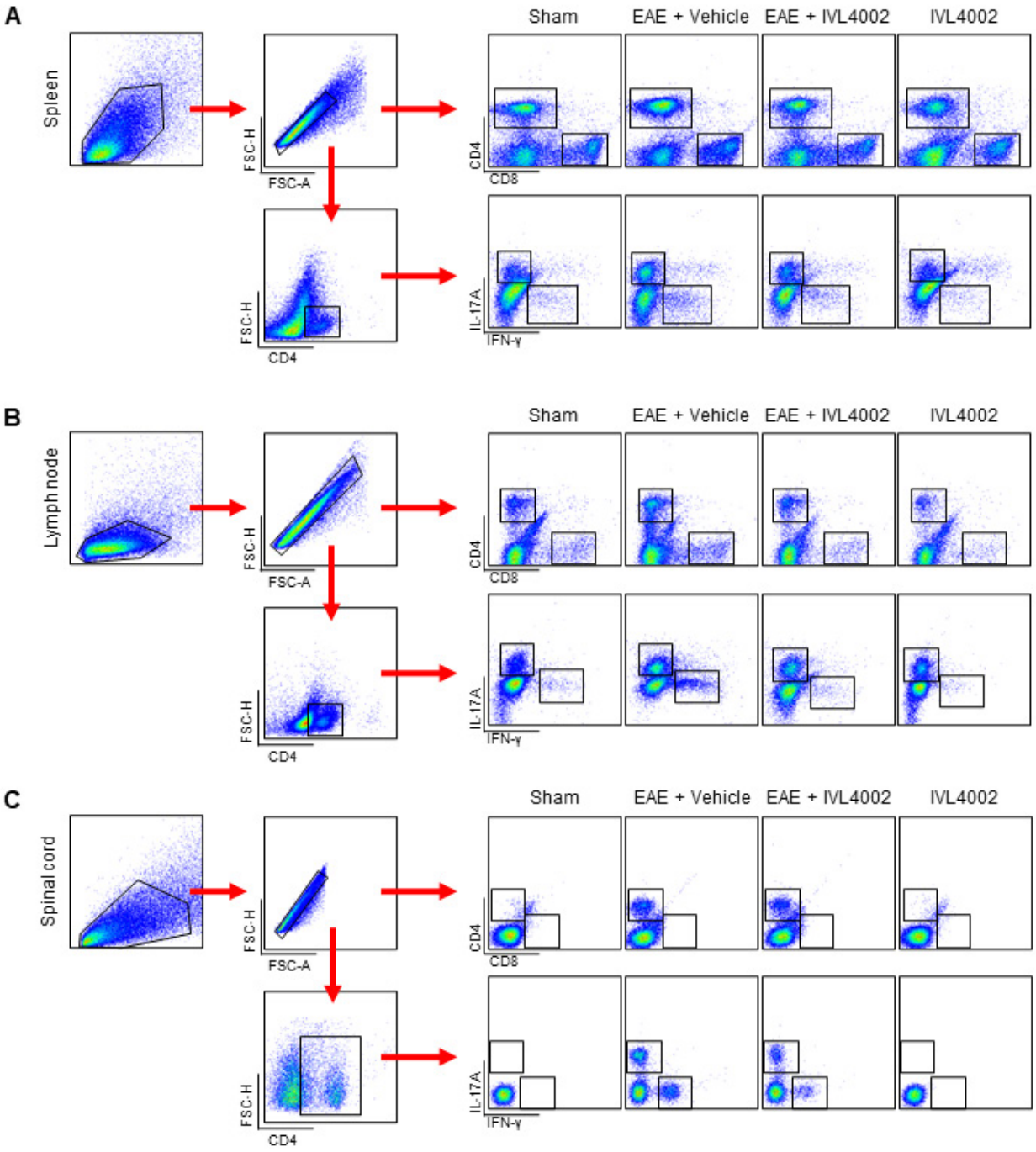


Figure S5. Flow cytometric gating strategy and representative dot plots corresponding to the T-cell subset quantification presented in Figure 5D–O. (A-C) Representative flow cytometric gating strategy used for the analysis of T-cell subsets. Single-cell suspensions were first gated using forward scatter (FSC-A) and side scatter (SSC-A) to exclude debris. Doublets were removed by FSC-H versus FSC-A gating. $CD4^+$ T cells

were subsequently identified, and intracellular staining for IFN-γ and IL-17A was performed to define Th1 ($CD4^+$ $IFN\text{-}\gamma^+$) and Th17 ($CD4^+$ $IL\text{-}17A^+$) populations. Representative dot plots from sham, EAE + vehicle, EAE + IVL4002, and IVL4002 groups are shown. Representative gating strategy and dot plots for T-cell subset analysis in spleen (A), draining lymph nodes (B) and spinal cord (C). Cells were sequentially gated based on FSC-A/SSC-A and doublet exclusion, followed by identification of $CD4^+$ T cells and intracellular detection of IFN-γ and IL-17A to define Th1 and Th17 populations, respectively.

Figure S6

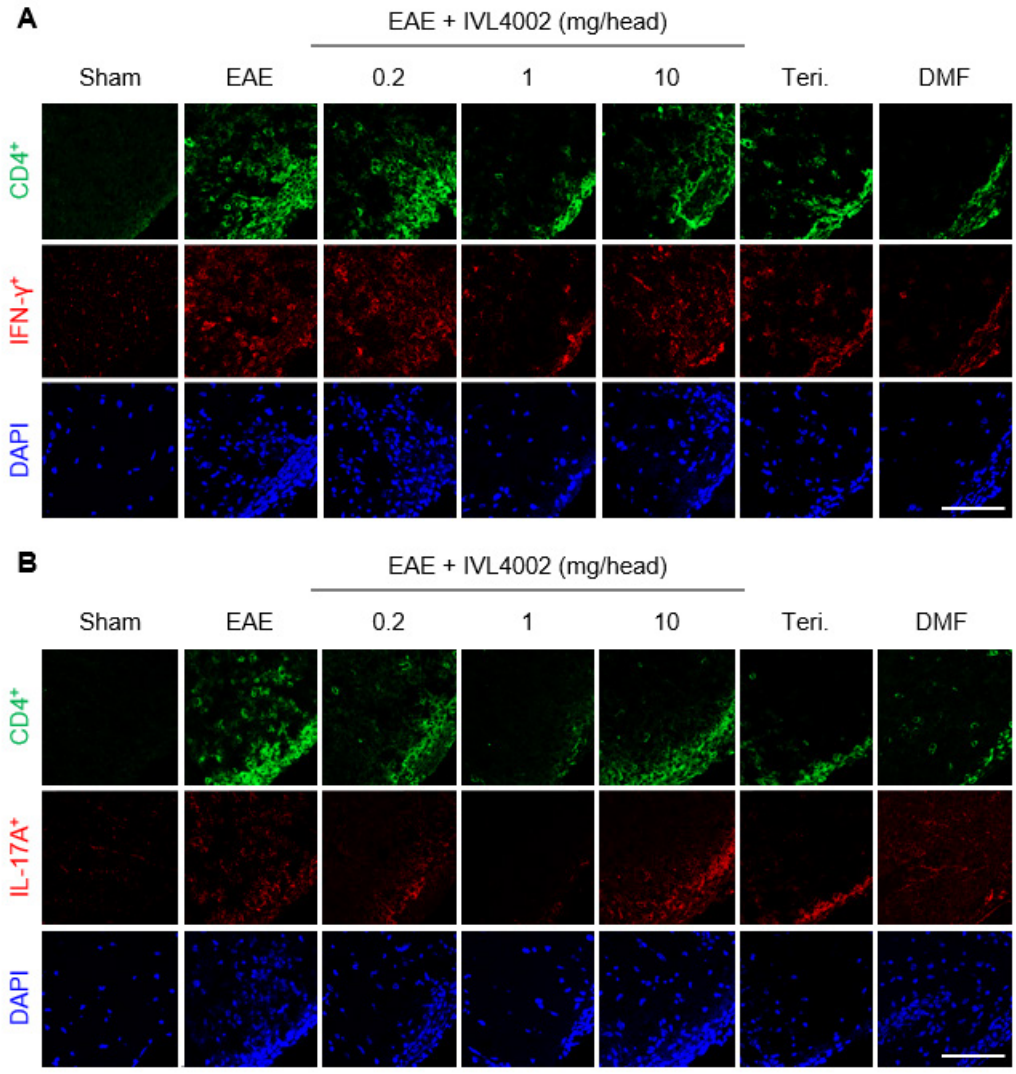


Figure S6. Single-channel images corresponding to the merged immunofluorescence images presented in Figure 5P. Representative single-channel images of CD4 (green), IFN-γ or IL-17A (red), and DAPI (blue) used to generate the merged images shown in Figure 5P. **(A)** CD4, IFN-γ, and DAPI channels. **(B)** CD4, IL-17A, and DAPI channels. Scale bar, 50 μm.

Figure S7

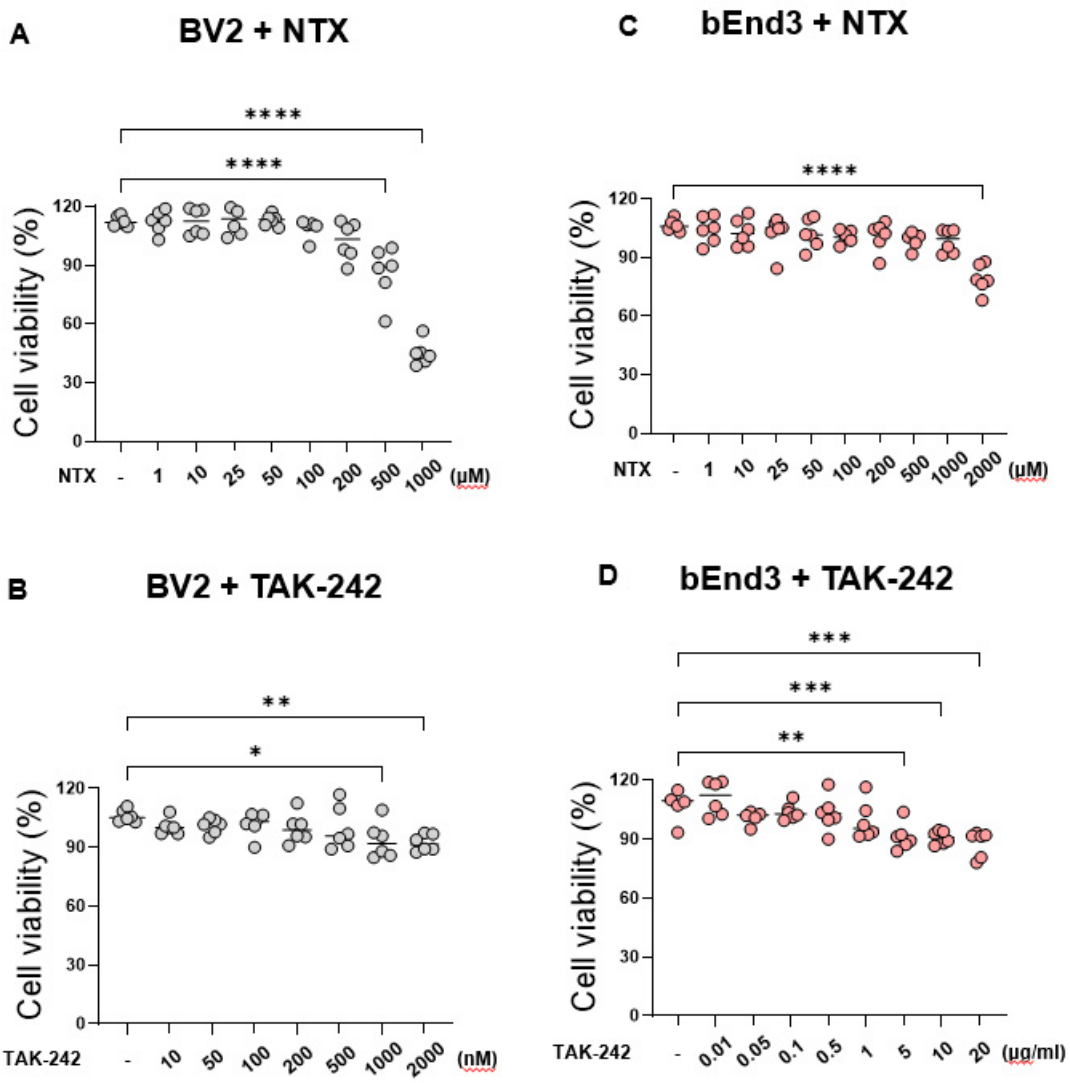


Figure S7. Effects of naltrexone and TAK-242 on the viability of BV2 microglial and bEnd.3 endothelial cells. BV2 and bEnd.3 cells were seeded at 1 × 10^4 cells per well and treated with the indicated concentrations

of naltrexone (NTX) or TAK-242 for 24 h, followed by assessment of cell viability using the MTT assay. (A, B) Viability of BV2 microglial cells treated with NTX (A) or TAK-242 (B). (C, D) Viability of bEnd.3 endothelial cells treated with NTX (C) or TAK-242 (D). Data are presented as the mean ± SEM. $P < 0.05$, *$P < 0.01$, **$P < 0.001$, and ***$P < 0.0001$ versus the untreated control.